LETTER Communicated by Majid Ghoshuni

Classification of Autism Spectrum Disorder from EEG-based Functional Brain Connectivity Analysis

Noura Alotaibi
nma1y17@soton.ac.uk
Koushik Maharatna
km3@ecs.soton.ac.uk
Department of Electronics and Computer Science, University of Southampton, Southampton, SO17 1BJ, U.K.

Autism is a psychiatric condition that is typically diagnosed with behavioral assessment methods. Recent years have seen a rise in the number of children with autism. Since this could have serious health and socioeconomic consequences, it is imperative to investigate how to develop strategies for an early diagnosis that might pave the way to an adequate intervention. In this study, the phase-based functional brain connectivity derived from electroencephalogram (EEG) in a machine learning framework was used to classify the children with autism and typical children in an experimentally obtained data set of 12 autism spectrum disorder (ASD) and 12 typical children. Specifically, the functional brain connectivity networks have quantitatively been characterized by graph-theoretic parameters computed from three proposed approaches based on a standard phase-locking value, which were used as the features in a machine learning environment. Our study was successfully classified between two groups with approximately 95.8% accuracy, 100% sensitivity, and 92% specificity through the trial-averaged phase-locking value (PLV) approach and cubic support vector machine (SVM). This work has also shown that significant changes in functional brain connectivity in ASD children have been revealed at theta band using the aggregated graph-theoretic features. Therefore, the findings from this study offer insight into the potential use of functional brain connectivity as a tool for classifying ASD children.

1 Introduction

Autism is a neurodevelopmental disorder characterized by lacks in social communication and language acquisition, in addition to restricted interests and repetitive behavior (Mohammad-Rezazadeh, Frohlich, Loo, & Jeste, 2016). According to the National Autistic Society report in 2016, around 700,000 people had the autism spectrum disorder (ASD) in the United Kingdom, and if we include their families, ASD is considered a part of daily life

Neural Computation **33, 1–27** (2021)
https://doi.org/10.1162/neco_a_01394

for 2.8 million people (National Autistic Society, 2016). Being incurable, this incurs extremely high cost to the social system in terms of health care, special education services, and losses in productivity (Buescher, Cidav, Knapp, & Mandell, 2014).

Early diagnosis is crucial for an adequate intervention, which also helps to improve the outcomes for affected children, allows them to receive proper care at an early stage, potentially prevents severe symptoms, and reduces the cost needed for the care of ASD children (Zwaigenbaum & Penner, 2018). A critical aspect of early diagnosis is to identify the underlying biomarkers to assess the risk even before the emergence of atypical behavioral symptoms (Zwaigenbaum & Penner, 2018). Characterization of task-specific functional brain connectivity has been considered a promising approach for identifying ASD biomarker as it reveals the information exchange patterns among different areas in the brain (Mohammad-Rezazadeh et al., 2016).

Functional brain connectivity is commonly measured by neuroimaging techniques such as electroencephalogram (EEG) and functional magnetic resonance imaging (fMRI). In a clinical application specifically for the diagnosis of brain disorders, a range of recent studies has begun to explore the utility of EEG in the detection of these disorders. Gurau, Bosl, and Newton (2017) provided a recent systematic review to examine the evidence for the efficiency of EEG signal analysis in ASD diagnoses. Their study classified EEG analysis methods into three classes: spectral power analysis, information dynamics, and functional brain connectivity. In particular, EEG-based functional connectivity can be categorized into information-based techniques, linear and nonlinear. Nonlinear functional connectivity methods are designed to detect the dynamic and nonstationary characteristic of EEG. Interacting chaotic oscillator-based phase synchronization is the most popular measure of nonlinear neural connectivity (Hamedi, Salleh, & Noor, 2016). It provides an amplitude-independent measure of connectivity between cortical regions and thus is less susceptible to the effects of artifacts and intertrial and intersubject amplitude variability (Hamedi et al., 2016). The most common phase synchronization methods used in neuroscientific literature are phase-locking value (PLV), phase-lag index (PLI), and weighted phase-lag index (WPLI) (Niso et al., 2013). Functional brain connectivity has gained increased attention in neuroscience as evidence suggests that phase-based connectivity analysis could reveal a task-dependent information exchange topography in the human brain, which could offer insight into pathological brain states.

The majority of explorations in the domain of adopting functional brain connectivity in detecting a disease state are focused on the field of detection of epileptic seizure (Le Van Quyenet al., 2005; Adebimpe, Aarabi, Bourel-Ponchel, Mahmoudzadeh, & Wallois, 2015), Parkinson's (Hassan et al., 2017), Alzheimer's (Tijms et al., 2013), attention deficit hyperactivity disorder (ADHD) (Janssen et al., 2017), and schizophrenia (Olejarczyk &

Jernajczyk, 2017). Compared to that, detailed exploration for using the change in the task-dependent functional connectivity to classify cognitive disorders such as ASD is not extensive. However, some studies observed correlations between changes in functional brain connectivity and ASD (Barttfeld et al., 2013; Ahmadlou & Adeli, 2017; Han et al., 2017). But such phenomenological evidence has yet to be brought into clinical practice.

The key idea in this letter is to analyze task-dependent functional brain connectivity to explore its potential for classifying ASD and typically developing (TD) children. More specifically, we use EEG-based functional brain connectivity owing to the EEG's noninvasiveness and ease of use, making the diagnostic process easily applicable in primary or secondary care. Our aim is to design a machine learning framework to classify children with ASD by applying PLV-based task-dependent brain connectivity and graph-theoretic measures to deduce the characteristics of the extracted brain's network. We are also seeking to find the most discriminating graph metrics (markers) to be used as the features for training a classification model. Since EEG is composed of five physiological frequency bands, we intend to identify the association between frequency bands and dysfunction in brain connectivity in children with ASD. Our methodology for classification ASD consists of several steps. First, the EEG signals are decomposed into five frequency bands. Then a connectivity map is formulated by three PLV approaches: trial-averaged PLV, averaged trial-averaged PLV, and time-points-averaged PLV. Each connectivity map is characterized by graph theory indices for every subject in each frequency band, and then graph-theoretic measures are used as features fed into classifiers for evaluating the proposed approaches in ASD classification.

The remainder of this letter is organized as follows: the description of the data set, the preprocessing techniques, the basic concept of PLV, and analysis procedures are described in section 2. The analysis of results is depicted in section 3 and discussed in section 4. The conclusion is presented in section 5.

2 Materials and Methods

2.1 Experimental Design and Data Preprocessing. The EEG data used in this study were obtained from Jamal et al. (2014) a modified data set from that obtained in Apicella, Sicca, Federico, Campatelli, & Muratori, (2013), which studied EEG characteristics in ASD and TD children with respect to face perception tasks. We selected it for this exploration because impairment in social processing is a core difficulty in ASD, which can be conveyed by emotions shown on the face, and this could be strictly connected to the disruption of the ability to activate specific brain circuits during face processing (Jamal et al., 2014).

The data were collected from 24 subjects: 12 children (7 boys and 5 girls) with ASD and 12 TD children (7 boys and 5 girls). Those in the ASD group

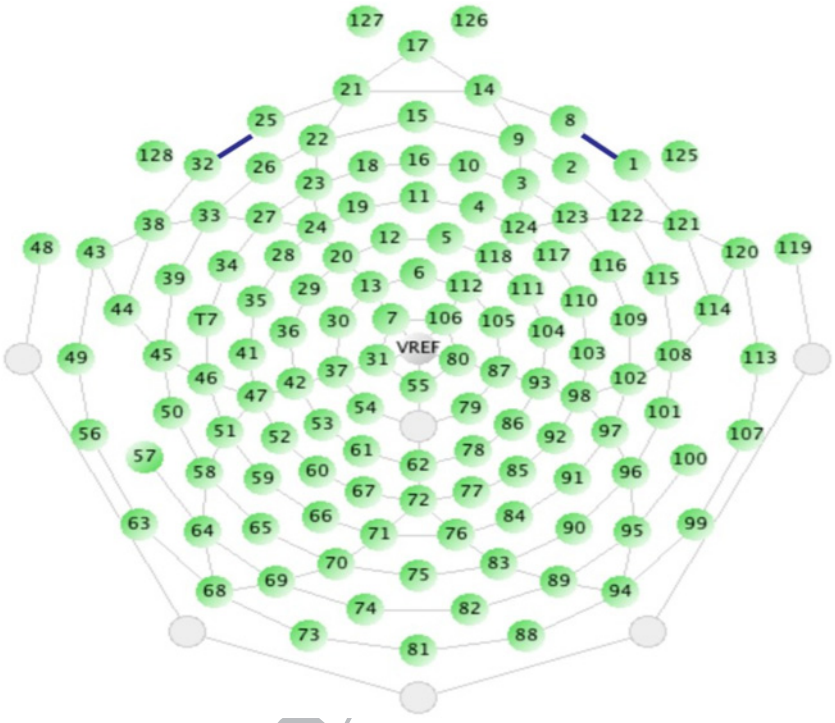

Figure 1: HydroCel Geodesic Sensor Net sensor layout (Apicella et al., 2013).

averaged 10.2 years old (range 6 to 13 years old), as did the control group 6 to 13 (mean 9.7) Faces with three types of emotion—happy, neutral, and fearful—were displayed for each subject during the EEG recording. The experiment consisted of three blocks each composed of 10 happy faces, 10 fearful faces and 10 neutral faces. Each stimulus was presented for 850 ms with an interstimulus interval of 150 ms. EEG data were recorded at 250 Hz using a 128channel HydroCel Geodesic Sensor Net, as shown in Figure 1 (Apicella et al., 2013).

The continuous EEGs were segmented into 1000 ms epochs (150 ms of baseline and 850 ms of stimulus presentation) a reasonable epoch length typically used in ERP research in order to capture the entire temporal dynamics of the ERP (Nam, Nijholt, & Lotte, 2018). Any segment containing signals above a threshold (200 μV) is contaminated by artifacts such as blinking or other eye movement was not used in further analysis (Jamal et al., 2014). Next, we used a second-order Butterworth bandpass filter to divide the EEG into its five traditional narrowband frequencies: delta (−4 Hz), theta (4–8 Hz), alpha (8–13 Hz), beta (13–30) and gamma (30–45)

(Wang, Sokhadze, El-Baz, Li, Sears, Casanova, & Tasman, 2016). These narrowband components were then subjected to PLV matrix calculation.

2.2 Computing PLV Matrix. PLV is a classical approach for quantifying phase synchronization, a key strategy for estimating functional brain connectivity. We chose it for this study because it is simple and fast to compute (Bruña, Maestú, & Pereda, 2018). The strength of phase synchronization is calculated by representing the absolute value of the mean of the phase difference between two signals (Aydore, Pantazis, & Leahy, 2013). The phase is often calculated using Hilbert or complex wavelet transform, and both approaches yielded the same result with the same efficiency (Bruña et al., 2018). PLV value ranges between zero and one—zero when the two signals are totally independent and one when the two signals are strongly coupled (Aydore et al., 2013). Mathematically, it is defined as

$$PLV = \left|\langle \exp(j\Delta\emptyset)\rangle\right|, \tag{2.1}$$

where $\Delta\emptyset$ denotes the phase difference between two signals and $\langle\,\rangle$ is an expectation operator (Brunner, Scherer, Graimann, Supp, & Pfurtscheller, 2006). Lachaux, Rodriguez, Martinerie, and Varela (1999) define PLV as a time-dependent measure to estimate the intertrial variability of phase at time t. Hence, equation 2.1 can be written as

$$PLV_t = \frac{1}{N}\left|\sum_{n=1}^{N} \exp(j\{\emptyset_1(t,n) - \emptyset_2(t,n)\})\right|, \tag{2.2}$$

where $\emptyset_i(t,n)$ is the instantaneous phase of signal $i \in \{1,2\}$ at time t and trial n, and N is a number of trials. The first step to calculate PLV is to compute the instantaneous phase $\emptyset(t)$. Here, we used the Hilbert transform for this purpose, which is defined as

$$\tilde{x}_i(t) = \frac{1}{\pi} PV \int_{-\infty}^{\infty} \frac{x_i(\tau)}{t-\tau} d\tau, \tag{2.3}$$

where $\tilde{x}_i(t)$ is the Hilbert transform of the original signal $x_i(\tau)$, and the transformation is calculated using integration of division of the original signal over the time shifted by τ (Brunner et al., 2006). PV is the Cauchy principal value, used to avoid errors in calculation due to improper integration. The instantaneous phase can then be calculated as

$$\emptyset(t) = arctan = \frac{\tilde{x}_{i(t)}}{x_i(t)}, \tag{2.4}$$

where $\emptyset(t)$ is the phase extracted from each time point $t[1, \ldots, T]$, trial $n[1, \ldots, N]$, and for each frequency band. On the completion of phase extraction, the exponentiation is calculated to obtain the unit phase difference vector between each pair of channels; hence, the series of phases difference vectors induce a connectivity matrix.

2.3 Connectivity Graph Formulation. Functional brain connectivity analysis has been applied to derived PLV matrix in this work. It is an established technique for gaining insight into the process of information propagation among the brain areas—the underpinning mechanism of the working principle of the brain. In this technique, the brain regions are represented as nodes of a graph, and the arcs (either weighted, directional or simply binary) between them represent the connection strengths between the nodes as derived from the PLV matrix.

The graph thus formed can be quantitatively characterized using a set of graph-theoretic parameters. Typically, these parameters could be categorized in two classes: node specific and network aggregate. The first one allows us to understand the property of one node in terms of its connectivity with the neighboring node (here, one brain region to the others), and the network aggregate features characterize the network as a whole in terms of ease of information flow along the network and any specialized local processing. Neuroimaging results suggest that ASD children have long-distance hypoconnection but short-distance hyperconnection (Kana, Uddin, Kenet, Chugani, & Muller, 2014). These two properties could be captured by a set of network aggregate features: transitivity is a feature to capture the characteristics of localized processing, characteristic path length, global efficiency, radius, and diameter, which capture the essence of information flow in the network. Therefore, in this work, we have chosen these five parameters because they are expected to adequately capture the essence of information flow disruptions in an ASD brain. Detailed descriptions of these parameters are given in Table 1.

2.4 Features Extraction. To extract the graph-theoretic features, we adopted three approaches for calculating the PLV matrix: trial-averaged PLV, averaged trial-averaged PLV, and time-points-averaged PLV.

2.4.1 Trial-Averaged PLV. The PLV connectivity matrix was computed between each pair of time series at a specific frequency, and the instantaneous phase is estimated at specific time points across the various trials. Therefore, at each time point t, the exponent of instantaneous phase difference was calculated between each pair of time series over trials N, and then the average phase differences across trials were obtained.

In equation 2.2, N is a total number of trials, t is a specific time point, n is a certain trial, and PLV_t indicates the connectivity matrix at time t. This process is repeated for each time point at each frequency band in each

Table 1: Detailed Description of Graph-Theoretical Features.

Feature Name	Description	Mathematical Description
Transitivity	It represents the ratio of the triangle to triplets in the network, and it measures a tendency of nodes to cluster together. The network with high transitivity contains groups of nodes that are densely connected internally. Finding such groups is very important because they reveal the functional modules.	$T = \frac{\sum_{i \in N} 2t_i}{\sum_{i \in N} k_i(k_i - 1)}$ where T is transitivity of the network, N is the set of all nodes in the network, k_i is a degree of node i, and t_i is the number of triangles around node i, which is calculated as follows: $t_i = \frac{1}{2} \sum_{j,h \in N} a_{ij} a_{ih} a_{jh}$, where a_{ij}, a_{ih}, a_{jh}, are connections between node i and j, i and h, and j and h, respectively. A degree of node i, k_i, is computed by $k_i = \sum_{j \in N} a_{ij}$.
Characteristic path length	It represents the average distance between all possible pairs of nodes in the network. It measures the network's ability to exchange information rapidly between distinct nodes.	$L = \frac{1}{N} \sum_{i \in N} L_i = \frac{1}{N} \sum_{i \in N} \frac{\sum_{j \in N, j \neq i} d_{ij}}{N - 1}$, where L_i is the average distance between node i and all other nodes, and d_{ij} is the shortest path length (distance) between nodes i and j. It is mathematically described as $d_{ij} = \sum_{a_{st} \in l_{i \leftrightarrow j}} a_{st}$, where $l_{i \leftrightarrow j}$ is the shortest path between node i and node j, which means, in a weighted graph, the path with minimum weight link between node i and j.

Table 1: Continued.

Feature Name	Description	Mathematical Description
Global efficiency	It is the average of inverse shortest path length and is related to characteristic path length. It is an important measure in assessing the efficiency of the network by measuring the ability of parallel information exchanged across the whole network (Liu et al., 2017). Higher global efficiency refers to higher network efficiency in transferring information.	$E = \frac{1}{N}\sum_{i\in N} E_i = \frac{1}{N}\sum_{i\in N}\frac{\sum_{j\in N, j\neq i} d_{ij}^{-1}}{N-1}$, where E_i is the efficiency of the node i, and d_{ij}^{-1} is an inverse of the shortest path length.
Radius	It is a measure of network shape and is defined as the minimum of network eccentricity that could be described as the maximum distance between node i and any other nodes in the network. Eccentricity assesses the ability of integration of the network, and high eccentricity refers to a more integrated network (Fraga González et al., 2016).	$r = \min(e_i)$, where e_i is a network eccentricity for node i, and it refers to the maximum value of each row of the dot product of d_{ij}: $e_i = \max(d_{ij} \circ d_{ij})$.
Diameter	Another measure of network eccentricity, it is defined as the maximum value of eccentricity.	$D = \max(e_i)$.

stimulus. As a result, in each frequency band, we obtained M connectivity matrices where M is the number of time points (in this study, $M = 250$). Once connectivity networks were formulated (from each frequency band, in each stimulus, and for each subject separately), the graph-theoretic parameters were extracted from each network. These features were then used to train a set of classifiers, and their performance was analyzed. A block diagram for this approach is shown in Figure 2. This approach is applied because typically in an event-related experiment, the averaging process has been carried out over the trials to enhance the signal-to-noise ratio.

2.4.2 Averaged Trial-Averaged PLV. The connectivity matrix was estimated in the same manner as in the first approach with a slight difference: after getting N connectivity matrices, the average over N was calculated, ending up with one averaged connectivity matrix. Then the complex network was estimated, and the graph parameters were extracted from this network. Following that, the feature selection algorithm was run to find most of the discriminant information needed for our classification problem. Here, we employed the Fisher discriminant ratio as a criterion for ranking the features because it can quantify the ability for each individual feature in separation between classes (Theodoridis, Pikrakis, Koutroumbas, & Cavouras, 2010).

The features with high ranking have greater discriminability. FDR can be defined as a ratio between-class distance to scatter within class. Mathematically, it is computed based on the mean and variance of both classes as

$$FDR = \frac{(\mu_1 - \mu_2)^2}{(\sigma_1^2 + \sigma_2^2)}, \tag{2.5}$$

where μ_1 is the mean of the first class, μ_2 is the mean of the second class, σ_1^2 and σ_2^2 are the variances of the first and second class, respectively. The features were ranked by FDR, and the cross-correlations between the features were calculated as

$$\rho_{ij} = \frac{\sum_{n=1}^{N} x_{ni} x_{nj}}{\sqrt{\sum_{n=1}^{N} x_{ni}^2 \sum_{n=1}^{N} x_{nj}^2}}, \tag{2.6}$$

where x_{nk} is the kth feature of the nth pattern, and ρ_{ij} is the cross-correlation coefficient between features i and j (Theodoridis & Koutroumbas, 2008). The best discriminant features were selected using the following steps (Theodoridis & Koutroumbas, 2008):

1. The features were ranked in descending order according to FDR, and the feature with the best rank, say, x_{i_1}, was selected where i_1 was the index of the feature.

Figure 2: Schematic diagram of trial-averaged PLV. Each time series recording from each electrode is filtered by Hilbert transform to extracting instantaneous phase. Exponents of phase difference a_{ij} between each pair of time series i and j are computed at time points t_1 for each trial n, and these yield N matrices, (from $(t_1, 1)$ to (t_1, N)) where N is the number of trials. By averaging over trials N, we obtain PLV at t_1. Repeating this process for each time point yields T connectivity matrices representing a synchrony index that related to intertrial variability.

2. We computed the cross-correlation coefficient between x_{i_1} and the remaining features: $\rho_{i_1 j}$ where$i_1 \neq j$.
3. We chose the second feature (say, x_{i_2}) based on the following:

$$i_2 = arg\alpha_1 C(j) - \alpha_2 |\rho_{i_1 j}|\}, \text{ for all } j \neq i_1, \tag{2.7}$$

where α_1, α_2 are weighting factors and C is the class separability.

In this study, we considered the correlation as well as the class separability in the feature selection process. Prior to commencing the selection process, we calculated the normalization of features. It may be beneficial for removing bias due to features having a high value, and it may have a strong influence on the cost function used for designing the classifier (Theodoridis & Koutroumbas, 2008). The features were normalized to zero mean and unit variance according to

$$\hat{x}_i = \frac{x_i - \bar{x}}{\sigma}, \quad i = 1, 2, \ldots, N, \tag{2.8}$$

where $\hat{x}_i$ is a normalized value, N is the number of features, x_i the feature i, $\bar{x}$ the mean, and σ the standard deviation. The schematic diagram for the trial-averaged approach is shown in Figure 3.

2.4.3 Time-Points-Averaged PLV. The connectivity index was computed between all pairs of time series for each specific trial at each frequency band. At each specific trial n, the exponentiation of the instantaneous phase difference was calculated between each pair of time series over the time points, and then the average of phase differences over the time points was estimated. The phase difference was computed by equation 2.2, where N is the number of time points, which here equals 250. This yields M connectivity matrices, each corresponding to one trial. Next, the average over the M matrices was computed, and we ended with one average matrix, mapped into the connectivity network.

In the final step, the graph parameters were inferred to find the most discriminant properties between the two populations. In the same way as in the second approach, we extracted the five features: transitivity, global efficiency, radius, diameter, and characteristic path length. The feature selection algorithm was then used to rank the features and select the most informative one for feeding into the classifier. The selection process proceeded in the same manner as in the second approach. This approach was proposed to investigate the variability of phase difference at trial n. If the phase difference slightly varies across the times, PLV is close to 1; otherwise, it is 0. The block diagram for the third approach is shown in Figure 4.

2.5 Classification. Different classification algorithms were trained with the selected features. Here, we evaluated the performance of SVM,

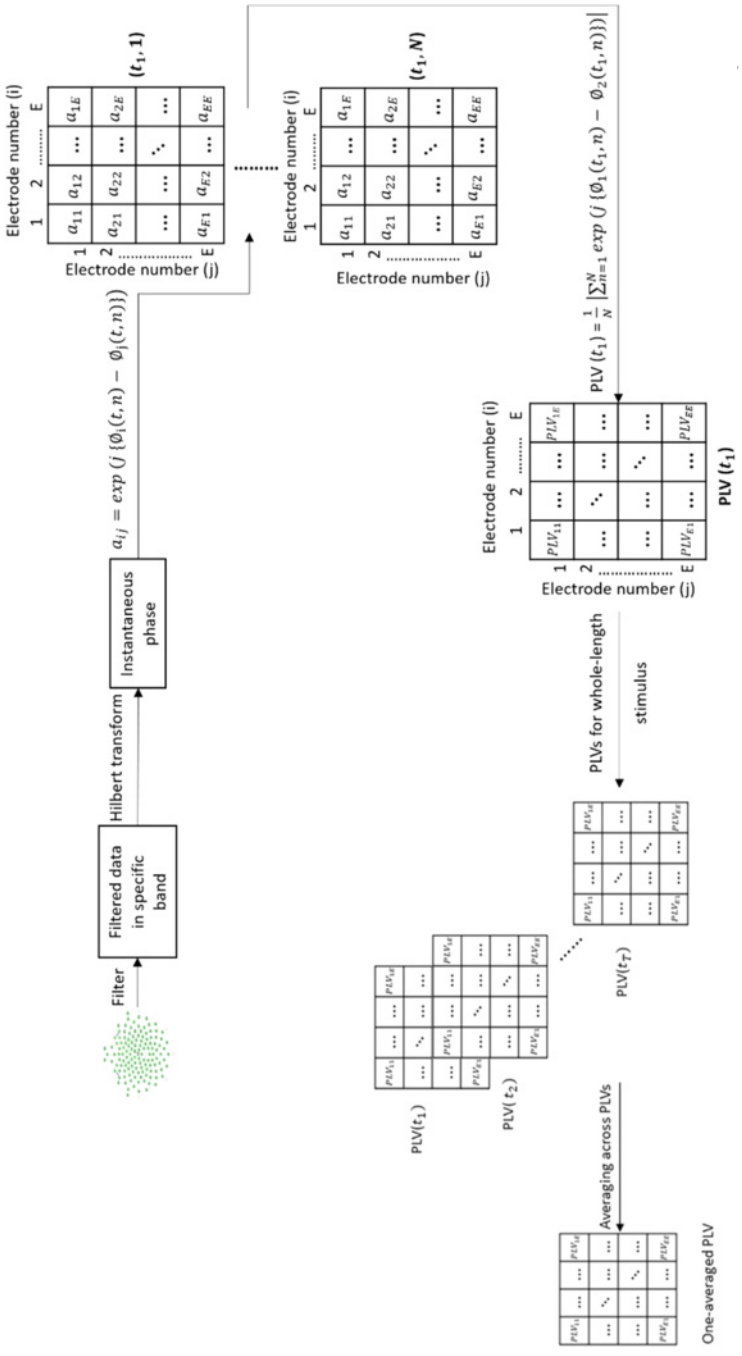

Figure 3: Schematic diagram of averaged trial-averaged PLV. Estimating PLV is carried out in the same manner as trial-averaged PLV with the difference in finalizing the estimation process by taking the average across the PLV matrices, and ending up with one PLV matrix.

Figure 4: Schematic diagram of time points averaged PLV. After extracting the instantaneous phase by Hilbert transform, the exponents of phase differences (a_{ij}) between each pair of electrodes i and j are computed at trial n_1 for each time point t. These yield T matrices (from $(1, n_1)$ to (Tn_1)), where T is the time points length. By averaging a over time points T, we obtain PLV at n_1. Repeating this process for each trial yields N connectivity matrices representing the synchrony index that related to the stability of phase synchronization over time.

decision trees, KNN, and discriminant analysis. Exploring different classifiers helped to determine which classifier is most suitable for our classification task.

The process of training classifiers was accomplished using the classification learner app within the statistics and machine learning toolbox in Matlab. One of the most common problems that affects the result of classification is data overfitting, that is, the model performs well on training data but classifies new data poorly. Overfitting occurs for a variety of reasons, including the limited amount of available data. One solution to this problem is reserving the part of the data set for testing in order to ensure the classifier can adequately work on new data. An example of this strategy is leave-one-out cross-validation (LOOCV), whereby the data are split into two groups: one for testing and the rest for training. The classifier is trained on the training data and tested on the data allocated for testing. This process is repeated for each sample of data, and results are averaged out to produce a single estimation (i.e., classification accuracy) (Uddin, Dajani, Voorhies, Bednarz, & Kana, 2017).

We measured the performance of the classifiers using three metrics: accuracy (ACC), sensitivity (SNS), and specificity (SPC). Accuracy measures the percentage of subjects who correctly classified as belonging to the correct class—either ASD or TD. Sensitivity represents the percentage of correctly classified ASD children as belonging to the ASD class, and it is known as a true positive rate (TPR), whereas specificity measures the proportion of TD that truly classified as typical and is known as a true negative rate (TNR). Mathematically, these measures are computed as follow:

$$\text{Sensitivity (TPR)} = \frac{TP}{P} \times 100\%, \tag{2.9}$$

$$\text{Specificity (TNR)} = \frac{TN}{N} \times 100\%, \tag{2.10}$$

$$\text{Accuracy} = \frac{Tp + TN}{P + N} \times 100\%, \tag{2.11}$$

where TP is a true positive, representing the number of children who are correctly classified as belonging to the ASD class, and P is a total number of instances of the ASD class. TN is a true negative, which refers to the number of children who are correctly classified as belonging to a typical class, and N is the total number of children in the typical class.

3 Results

The one controversial issue about PLV performance is its sensitivity to volume conduction. It is a key challenge that faces EEG-based brain connectivity. Since EEG is recorded through the electrodes, this does not provide

Table 2: Best Classification Performance with the Happy Stimulus Using Trial-Averaged PLV.

Band	Accuracy	Sensitivity	Specificity	Classifier
Delta	83.3%	83%	83%	Fine tree
Theta	95.8%	100%	92%	Cubic SVM
				Fine KNN
Alpha	79.2%	75%	83%	Fine tree
Beta	79.2%	75%	83%	Medium gaussian SVM
Gamma	79.2%	83%	75%	Cubic SVM

The shaded row represents the highest classification performance.

direct access to the source signal. The electrodes record the linear and spontaneous superposition of multiple sources in the brain, and this may yield a spurious connectivity due to the electromagnetic field generated by the source in the brain (Cohen, 2014). The volume conduction is typically reflected as zero-phase; however, in our analysis, we investigated the zero-phase difference between each spatially closed pair of the electrodes as to mitigate the effects of volume conduction. The results of proposed approaches follow.

3.1 Trial-Averaged PLV. The features are generated from five network parameters, 250 connectivity matrices, five frequency bands, and three stimuli. To identify which graph-theoretic parameters are most powerful in distinguishing between the two populations, we formulated the features pools through all possible parameters' combinations. We ended up with 31 different cases in each frequency band.

Since we investigated five frequency bands in each stimulus, we had (31×5) cases in each stimulus. All of these cases have been fed into the various classifiers described in the previous section. Tables 2 to 4 show the best classification performance for each frequency band for each stimulus (happy, fearful, and neutral). By using LOOCV, we achieved the best classification accuracy of 95.8% using cubic SVM with a happy stimulus within the theta band for features combination between transitivity, global efficiency, radius, and diameter, with corresponding sensitivity and specificity of 100% and 92%, respectively.

We obtained the same classification accuracy by the fine KNN classifier in combinations of all features and combinations of radius, diameter, and characteristic path length. In addition, a difference between the ASD and TD groups was also observed in the delta band for the happy stimulus. A classification accuracy up to 83.3% was achieved with the fine tree classifier for multiple cases of feature combinations: combination of all features; combination of radius and diameter only; combination between transitivity, radius, and diameter; combination of global efficiency, radius, and

Table 3: Best Classification Performance with Fear Stimulus Using Trial-Averaged PLV.

Band	Accuracy	Sensitivity	Specificity	Classifier
Delta	75%	75%	75%	Cubic SVM
		75%	75%	Quadratic SVM
		67%	83%	Medium gaussian SVM
		83%	67%	Quadratic SVM
Theta	79.2%	75%	83%	Cubic SVM
Alpha	75%	83%	67%	Fine gaussian SVM
		75%	75%	Tree
Beta	70.8%	67%	75%	Tree
Gamma	79.2%	75%	83%	Fine KNN
		83%	75%	Fine KNN

The shaded rows represent the highest classification performance.

Table 4: Best Classification Performance with Neutral Stimulus Using Trial-Averaged PLV.

Band	Accuracy	Sensitivity	Specificity	Classifier
Delta	83.3%	83%	83%	Fine KNN
		92%	75%	
Theta	87.5%	92%	83%	Quadratic SVM
Alpha	83.3%	83%	83%	Cubic SVM
Beta	79.2%	75%	83%	Cubic SVM
Gamma	75%	75%	75%	Weighted KNN
		75%	75%	Cosine KNN
		67%	83%	Tree
		83%	67%	Fine gaussian SVM

The shaded rows represent the highest classification performance.

diameter; and combination of transitivity, global efficiency, and diameter. Hence, we can conclude for the happy stimulus that the best classification accuracy was achieved within the theta and delta bands.

In the fear stimulus, the optimal classification performance was observed in the theta and gamma bands with the medium gaussian SVM and fine KNN classifiers, respectively. However, classification accuracy does not exceed 79.2%, which was obtained within the theta band in case the diameter was a feature, with 67% sensitivity and 92% specificity, and for a combination of transitivity and global efficiency with 75% sensitivity and 83% specificity. In the gamma band, the best accuracy was observed for the combination of transitivity and global efficiency and that of transitivity and characteristic path length, with corresponding sensitivity and specificity of 83% and 75%, respectively, as well as for the case of characteristic path length, with 75% sensitivity and 83% specificity. Briefly, in the fear

stimulus, the difference between the two groups was revealed in the theta and gamma bands.

In the neutral stimulus, the best classification performance was obtained in the theta band with a classification accuracy up to 87.5%, along with 92% sensitivity and 83% specificity. This result was observed for a combination of transitivity, global efficiency, and diameter; a combination of transitivity, diameter, and characteristic path length; and a combination of global efficiency, diameter, and characteristic path length with quadratic SVM.

3.2 Averaged Trial-Averaged PLV. The feature pool was generated from five graph metrics and one averaged connectivity matrix; hence, it consisted of only five features. Here, we applied the feature selection algorithm to rank features by how informative they are. In each frequency band and corresponding to a single stimulus, we investigated the combination of features based on FDR ranking. In other words, we first examined the performance of the combination of the two highest-ranked features, then the three highest-ranked features, and so on. Consequently, we have 20 different cases in each stimulus, each evaluated through feeding it into a classifier to determine which feature set is optimal, with which frequency band, and with which stimulus.

The cases involve three stimuli, the possible combination of the highest-ranking five network parameters and five frequency bands. For example, the cases examined with the happy stimulus in the delta band were (transitivity and global efficiency), (transitivity, global efficiency, and radius), (transitivity, global efficiency, radius, and characteristic path length), and (transitivity, global efficiency, radius, characteristic path length, and diameter). Thus, the overall number of cases investigated in each stimulus within a specific frequency band was four.

The rankings of the set of five features investigated in each frequency band and corresponding to each stimulus are shown in Figures 5 to 7, and the best classification performances in each stimulus and within each frequency band are demonstrated in Figure 8. Under this approach, the best classification accuracy was 87.5%, with 83% sensitivity and 92% specificity. This classification performance was observed in the theta band within the happy stimulus using the fine KNN classifier with a combination of all five features. The same classification accuracy with 100% sensitivity and 75% specificity was realized with a neutral stimulus in the theta band using the quadratic SVM classifier with a combination of global efficiency, transitivity, and characteristic path length. For the fear stimulus, the optimal classification performance was observed in the alpha band, achieving 83.3% accuracy, 83% sensitivity, and 83% specificity using the quadratic SVM classifier with a combination of global efficiency, transitivity, and characteristic path length. In sum, this approach achieved reasonable results in the theta band within the happy and the neutral stimuli.

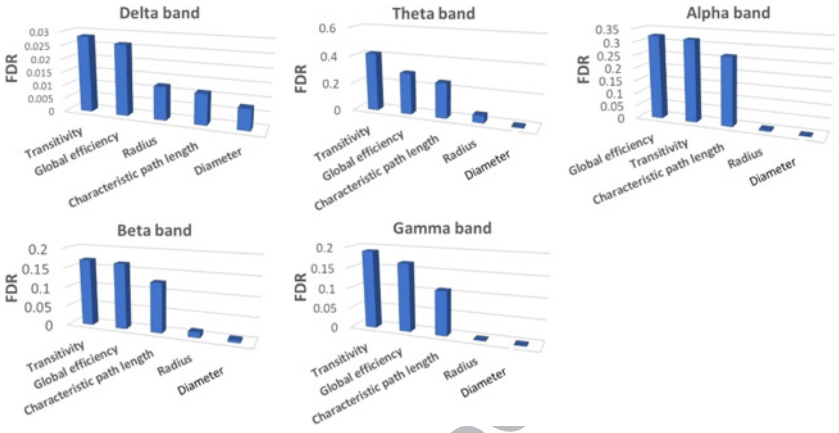

Figure 5: FDR ranking of five features in each frequency band with the happy stimulus using the averaged trial-averaged PLV approach.

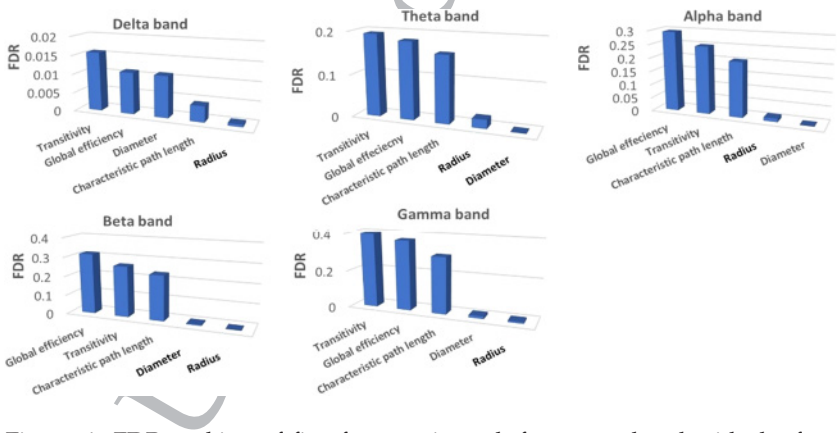

Figure 6: FDR ranking of five features in each frequency band with the fear stimulus using the averaged trial-averaged PLV approach.

3.3 Time-Points-Averaged PLV. The feature pool contained five features, ranked using FDR. In a similar manner to the second approach, we investigated the 60 cases to find the best features combination, frequency band, and stimulus that could capture the difference between the ASD and TD groups. Figures 9 to 11 show the ranking of the five parameters assessed in each frequency band for each stimulus, and the best performances in each stimulus within each band are depicted in Figure 12.

The best classification performance was realized on the fear stimulus in the alpha band using the tree classifier. This result, achieved with a

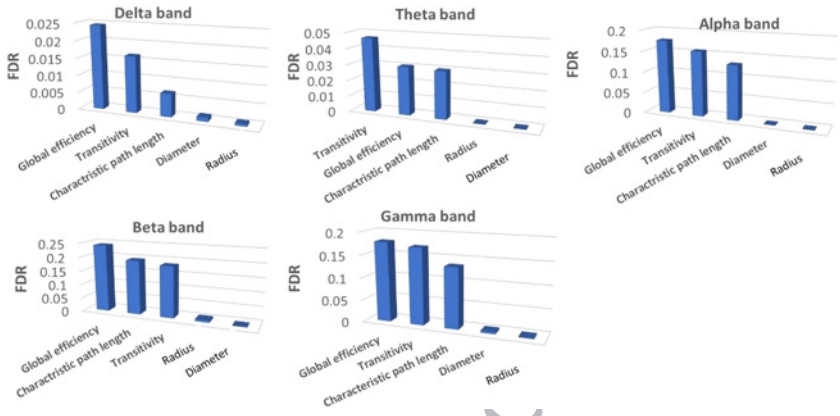

Figure 7: FDR ranking of five features in each frequency band with the neutral stimulus using the averaged trial-averaged PLV approach.

combination of all features, was 83.3% in terms of classification accuracy, with 75% sensitivity and 92% specificity. For the happy stimulus, classification accuracy did not exceed 75% in the theta band with a combination of all features. Sensitivity and specificity were 92% and 58%, respectively. Furthermore, the same accuracy was achieved in the delta band with 83% sensitivity and 67% specificity, with a combination of characteristic path length and diameter. By neutral stimulus, the classification performance did not exceed 75% in the alpha and beta bands.

4 Discussion

This study has characterized the difference in task-dependent functional brain network with ASD and TD. The aggregated graph-theoretic features have been used to train and test a set of supervised machine learning algorithms for classification between ASD and TD, and promising results have been achieved. These results demonstrate the potential superiority of classification performance over a state of art studies, as summarized in Table 5.

Kang, Han, Song, Niu, and Li (2020) recorded an EEG sample of 49 children with ASD and 48 controls, and features were extracted through two methods: power spectral density and eye tracking. Their results showed that the highest classification accuracy reached 85.44% using SVM. Abdolzadegan, Moattar, and Ghoshuni (2020) explored a set of linear and nonlinear features along with a set of feature selection criteria for early classification of children with ASD, and it has been validated on a data set of 34 children with ASD and 11 typical children. Their study achieved a high classification accuracy using SVM up to 90.57% and 99.91% as

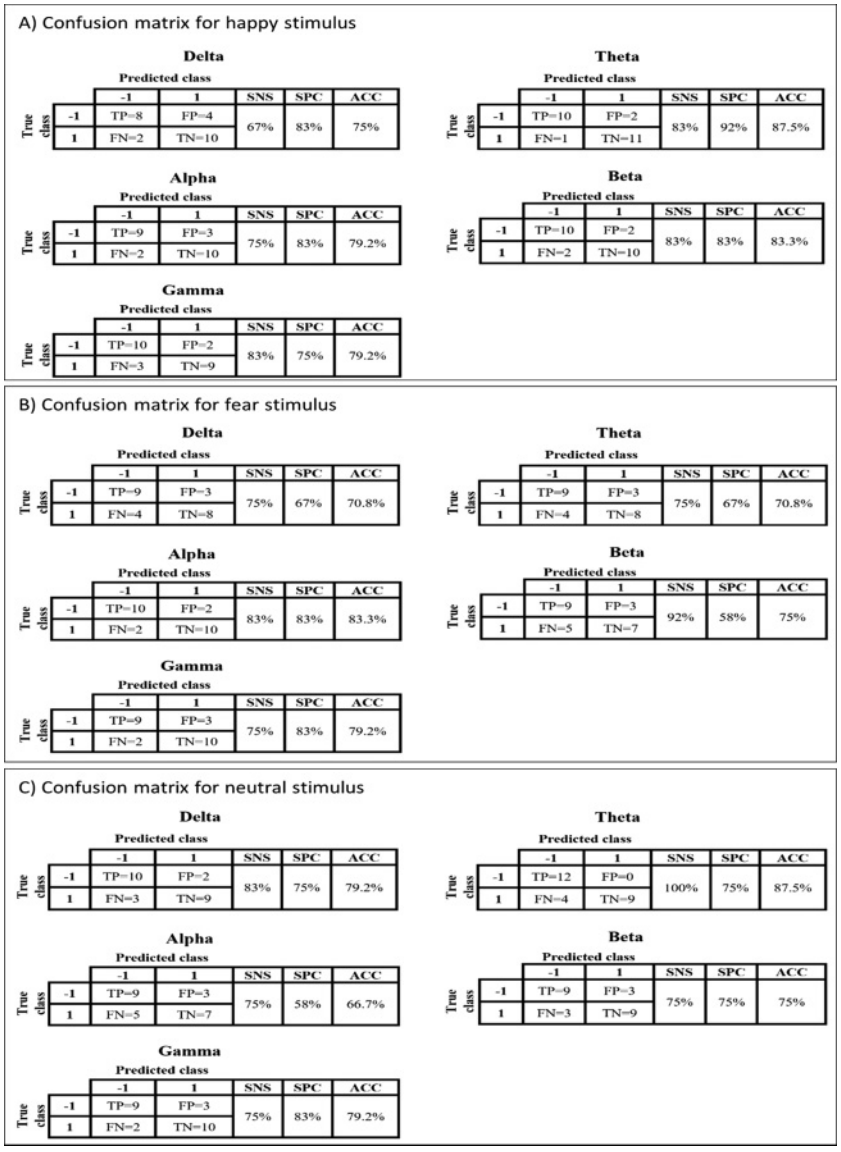

Figure 8: Confusion matrices of the best classification performance by averaged trial-averaged PLV. Panels A, B, and C show the results in each frequency band from happy, fear, and neutral stimuli, respectively.

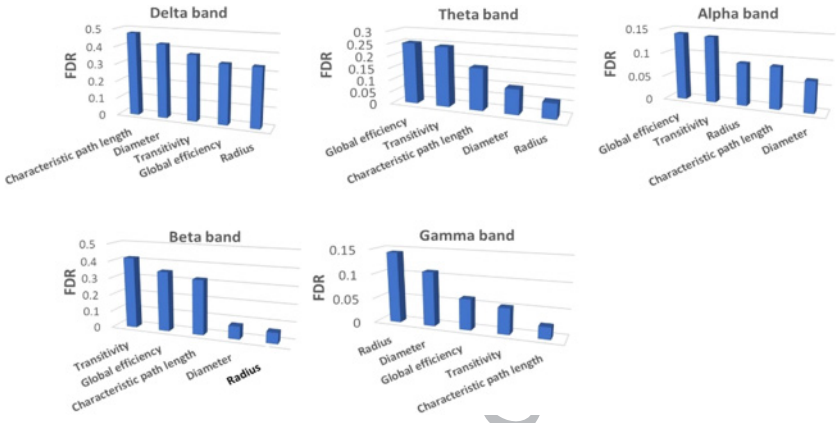

Figure 9: FDR ranking of five features in each frequency band with happy stimulus using time-points-averaged PLV.

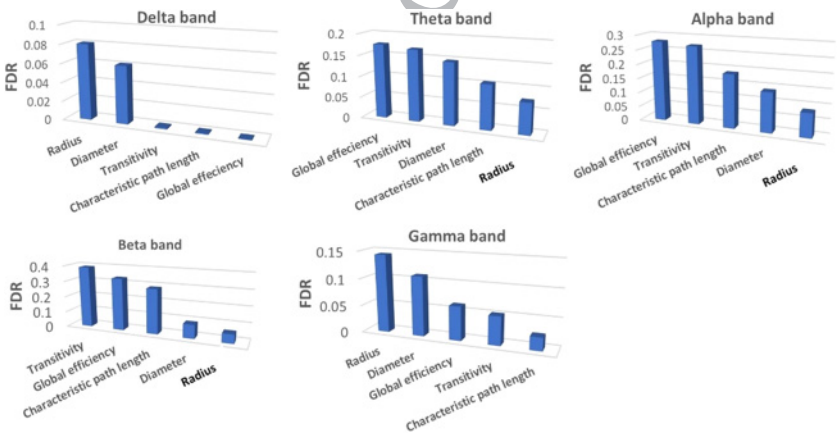

Figure 10: FDR ranking of five features in each frequency band with fear stimulus using time-points-averaged PLV approach.

sensitivity. Jayawardana, Jaime, and Jayarathna (2019) used a power spectrum and conventional neural network (CNN) to achieve classification accuracy up to 95%. Grossi, Olivieri, and Buscema (2017) conducted a study using a complex EEG analysis algorithm called multiscale ranked organizing map coupled with implicit function as a squashing time algorithm (MSROM/I-FAST) to extract the features for diagnosis autistic children along with a set of machine learning algorithms and achieving classification accuracy that reached 92.8% with random forest classifier. Ahmadlou,

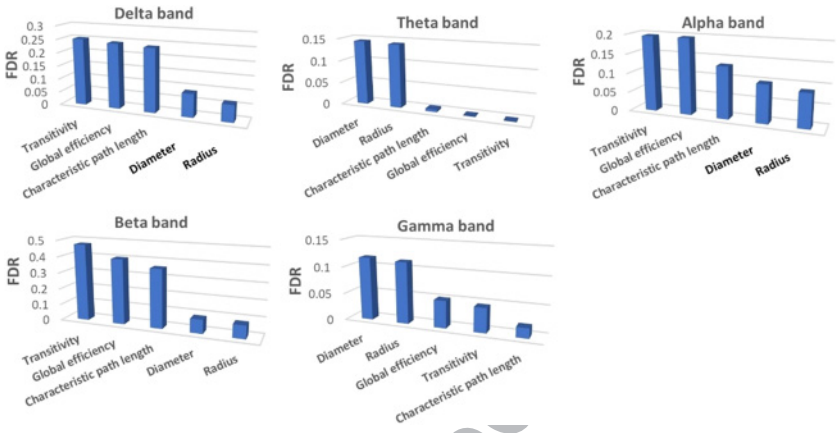

Figure 11: FDR ranking of five features in each frequency band with neutral stimulus using time-points-averaged PLV approach.

Adeli, and Adeli (2012) used fuzzy synchronization likelihood to classify autistic children, and it has been validated using a data set with nine autistic children and nine normal in a resting-state condition by applying an enhanced probabilistic neural network (EPNN). The classification accuracy was 95.5%.

Jamal et al. (2014) investigated our data set for classifying children with ASD and TD based on synchrostate analysis; the overall result was 94.7% accuracy for the classifier. A synchrostate has been derived from a high-density EEG system, which makes it not applicable to young children. In contrast, our approach (PLV) can be perfectly estimated by considering only a limited number of channels. PLV is used here to calculate phase synchronization between each pair of channels and analyzed this index based on graph theory parameters. It has several advantages, including fast and reliable calculation and its mathematical simplicity (Bruna et al., 2018).

One of the key findings of this study is that the significant difference between both populations was observed in the theta and alpha bands. This may be due to the activity of the theta band, usually associated with cognitive and emotional processing, and modulations of alpha band have been related to memory maintenance. In this context, some studies consistently report a close and strong association between alteration of theta and alpha oscillations and the subject with ASD. Li, Yan, and Wei (2013) have identified a relation between the theta band and working memory performance, while theta power increases and alpha power decreases, after an increase in task demands, such as the presentation of less frequent target stimuli in an oddball paradigm like the experimental paradigm shown in this study. Klimesch (1999) also proved that there were changes in the alpha and theta

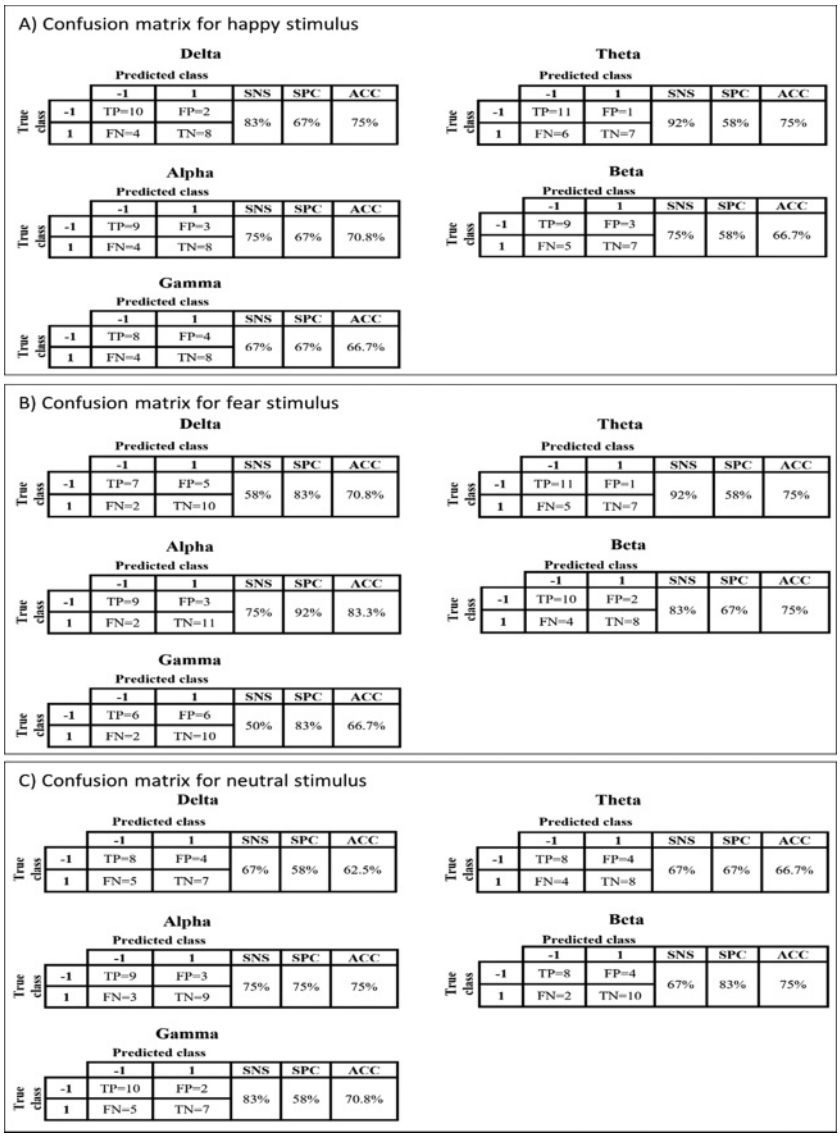

Figure 12: Confusion matrices of best classification performance by time-points-averaged PLV. Panels A, B, and C show the results in each frequency band from happy, fear, and neutral stimuli, respectively.

Table 5: Comparative Studies of EEG-Based Machine Learning for Diagnosis of Autism.

	Data Set						
Author	ASD	Age	TD	Age	Features Extraction	Classifier	Accuracy
Kang et al., 2020	49	3–6	48	3–6	Combination of power spectrum and eye-tracking data	SVM	85.44%
Abdolzadegan et al., 2020	34	3–12	11	3–12	Power spectrum, wavelet transform, FFT, fractal dimension, correlation dimension, Lyaptunov exponent, DFA, and entropy	SVM	90.75%
Jayawardana et al., 2019	8	5–17	9	6–16	Power spectrum	CNN	92.00%
Grossi et al., 2017	15	7–14	10	7–12	MSROM/I-FAST	random forest	92.80%
Jamal et al., 2014	12	6–13	12	6–13	Graph-theoretical parameters derived from synchrostate	SVM	94.70%
Ahmadlou et al., 2012	9	7–13	9	7–13	Fuzzy synchronization likelihood	EPNN	95.50%
Our study	12	6–13	12	6–13	Graph-theoretical parameters derived from PLV	SVM	95.80%

bands in subjects with a variety of neurological disorders when the subjects tried to respond to external stimuli. Moreover, a significant difference between ASD and TD subjects has been found in the alpha and theta bands based on Larrain-Valenzuela et al. (2017). In addition to these findings, our results showed that the network-aggregated measures derived from PLV can effectively classify both groups. However, we cannot generalize which is the most discriminative feature because the optimal graph metrics vary between PLV approaches and the types of stimuli.

5 Conclusion

The analysis of task-dependent functional brain connectivity successfully distinguishes between ASD and TD children using graph-theoretic features within a machine learning framework. The result of this investigation showed that trial-averaged PLV achieved a high classification accuracy, up to 95.8% by cubic SVM. Another obvious research finding that emerges from this study is that the difference between the two groups has been detected in the theta and alpha bands. Further research is recommended to confirm the effectiveness of methodology with large sample size.

References

Abdolzadegan, D., Moattar, M. H., & Ghoshuni, M. (2020). A robust method for early diagnosis of autism spectrum disorder from EEG signals based on feature selection and DBSCAN method. *Biocybernetics and Biomedical Engineering*, *40*, 482–493. doi:10.1016/j.bbe.2020.01.008

Adebimpe, A., Aarabi, A., Bourel-Ponchel, E., Mahmoudzadeh, M., & Wallois, F. (2015). Functional brain dysfunction in patients with benign childhood epilepsy as revealed by graph theory. *PLoS One*, *10*, 1–14. doi:10.1371/journal.pone.0139228

Ahmadlou, M., & Adeli, H. (2017). Complexity of weighted graph: A new technique to investigate structural complexity of brain activities with applications to aging and autism. *Neuroscience Letters*, *650*, 103–108. doi:10.1016/j.neulet.2017.04.009

Ahmadlou, M., Adeli, H., & Adeli, A. (2012). Fuzzy aynchronization likelihood-wavelet methodology for diagnosis of autism spectrum disorder. *Journal of Neuroscience Methods*, *211*, 203–209. doi:10.1016/j.jneumeth.2012.08.020

Apicella, F., Sicca, F., Federico, R. R., Campatelli, G., & Muratori, F. (2013). Fusiform gyrus' responses to neutral and emotional faces in children with autism spectrum disorders: A high density ERP study. *Behavioural Brain Research*, *251*, 155–162. doi:10.1016/j.bbr.2012.10.040

Aydore, S., Pantazis, D., & Leahy, R. M. (2013). A note on the phase locking value and its properties. *NeuroImage*, *74*, 231–244. doi:10.1016/j.neuroimage.2013.02.008

Barttfeld, P., Amoruso, L., 377 Ais, J., Cukier, S., Bavassi, L., Tomio, A., . . . Sigman, M. (2013). Organization of brain networks governed by long-range connections index autistic traits in the general population. *Journal of Neurodevelopmental Disorders*, *5*, 16. doi:10.1186/1866-1955-5-16

Bruña, R., Maestú, F., & Pereda, E. (2018). Phase locking value revisited: Teaching new tricks to an old dog. *Journal of Neural Engineering*, *15*, 056011. doi:10.1088/1741-2552/aacfe4

Brunner, C., Scherer, R., Graimann, B., Supp, G., & Pfurtscheller, G. (2006). Online control of a brain-computer interface using phase synchronization. *IEEE Transactions on Biomedical Engineering*, *53*, 2501–2506. doi:10.1109/TBME.2006.881775

Buescher, A. V. S., Cidav, Z., Knapp, M., & Mandell, D. S. (2014). Costs of autism spectrum disorders in the United Kingdom and the United States. *JAMA Pediatrics*, *168*, 721. doi:10.1001/jamapediatrics.2014.210

Cohen, M. X. (2014). *Analyzing neural time series data: Theory and practice*. Cambridge, MA: MIT Press.

Fraga González, G., Van der Molen, M., Žarić, G., Bonte, M., Tijms, J., Blomert, L., . . . Van der Moplen, M. W. (2016). Graph analysis of EEG resting state functional networks in dyslexic readers. *Clinical Neurophysiology*, *127*, 3165–3175. doi:10.1016/j.clinph.2016.06.023

Grossi, E., Olivieri, C., & Buscema, M. (2017). Diagnosis of autism through EEG processed by advanced computational algorithms: A pilot study. *Computer Methods and Programs in Biomedicine*, *142*, 73–79. doi:10.1016/j.cmpb.2017.02.002

Gurau, O., Bosl, W. J., & Newton, C. R. (2017). How useful is electroencephalography in the diagnosis of autism spectrum disorders and the delineation of subtypes? A systematic review. *Frontiers in Psychiatry*, *8*. doi:10.3389/fpsyt.2017.00121

Hamedi, M, Salleh, Sh-H., & Noor, A. M. 2016. Electroencephalographic motor imagery brain connectivity analysis for BCI: A review. *Neural Computation*, *28*(6), 999–1041. https://doi.org/10.1162/NECO_a_00838.

Han, J., Zeng, K., Kang, J., Tong, Z., Cai, E., Chen, H., . . . Li, X. (2017). *Development of brain network in children with autism from early childhood to late childhood*. *Neuroscience*, *367*, 134–146. doi:10.1016/j.neuroscience.2017.10.015

Hassan, M., Chaton, L., Benquet, P., Delval, A., Leroy, C., Plomhause, L., . . . Dujardin, K. (2017). Functional connectivity disruptions correlate with cognitive phenotypes in Parkinson's disease. *NeuroImage Clinical*, *14*, 591–601. doi:10.1016/j.nicl.2017.03.002

Jamal, W., Das, S., Oprescu, I.-A., Maharatna, K., Apicella, F., & Sicca, F. (2014). Classification of autism spectrum disorder using supervised learning of brain connectivity measures extracted from synchrostates. *Journal of Neural Engineering*, *11*, 46019. doi:10.1088/1741-2560/11/4/046019

Janssen, T. W. P., Hillebrand, A., Gouw, A., Gelade, K., Mourik, R. V., Maras, A., & Oosterlaan, J. (2017). Neural network topology in ADHD: Evidence for maturational delay and default-mode network alterations. *Clinical Neurophysiology*, *128*, 2258–2267. doi:10.1016/j.clinph.2017.09.004

Jayawardana, Y., Jaime, M., & Jayarathna, S. (2019). Analysis of temporal relationships between ASD and brain activity through EEG and machine learning. In *Proceedings of the IEEE 20th International Conference on Information Reuse and Integration for Data Science* (pp. 151–158). Piscataway, NJ: IEEE.

Kana, R. K., Uddin, L. Q., Kenet, T., Chugani, D., & Muller, R.-A. (2014). Brain connectivity in autism. *Frontiers in Human Neuroscience*, *8*, 8–11. doi:10.3389/fnhum.2014.00349

Kang, J., Han, X., Song, J., Niu, Z., & Li, X. (2020). The identification of children with autism spectrum disorder by SVM approach on EEG and eye-tracking data. *Computers in Biology and Medicine*, *120*. doi:10.1016/j.compbiomed.2020.103722

Klimesch, W. (1999). EEG alpha and theta oscillations reflect cognitive and memory performance: A review and analysis. *Brain Research Reviews*, *29*, 169–195. doi:10.1016/S0165-0173(98)00056-3

Lachaux, J. P., Rodriguez, E., Martinerie, J., & Varela, F. J. (1999). Measuring phase synchrony in brain signals. *Human Brain Mapping*, *8*, 194–208.

Larrain-Valenzuela, J., Zamorano, F., Soto-Icaza, P., Carrasco, X., Herrera, C., Daiber, F., . . . Billeke, P. (2017). Theta and alpha oscillation impairments in autistic spectrum disorder reflect working memory deficit. *Scientific Reports*, *7*, 1–11. doi:10.1038/s41598-017-14744-8

Le Van Quyen, M., Soss, J., Navarro, V., Robertson, R., Chavez, M., Baulac, M., & Martinerie, J. (2005). Preictal state identification by synchronization changes in long-term intracranial EEG recordings. *Clinical Neurophysiology*, *116*, 559–568. doi:10.1016/j.clinph.2004.10.014

Li, X., Yan, Y., & Wei, W. (2013). Identifying patients with poststroke mild cognitive impairment by pattern recognition of working memory load-related ERP. *Computational and Mathematical Methods in Medicine*, *2013*, 1–10. doi:10.1155/2013/658501

Liu, J., Li, M., Pan, Y., Lan, W., Zheng, R., Wu, F.-X., & Wang, J. (2017). Complex brain network analysis and its applications to brain disorders: A survey. *Complexity*, *2017*, 1–27. doi:10.1155/2017/8362741

Mohammad-Rezazadeh, I., Frohlich, J., Loo, S. K., & Jeste, S. S. (2016). Brain connectivity in autism spectrum disorder. *Current Opinion in Neurology*, *29*, 137–147.

Nam, C., Nijholt, A., Lotte, F. (Eds.), (2018). *Brain-computer interfaces handbook: Technological and theoretical advances*. Boca Raton, FL: CRC Press.

National Autistic Society (2016). *Autism*. https://www.autism.org.uk/about.aspx

Niso, G., Bruña, R., Pereda, E., Gutiérrez, R., Bajo, R., Maestú, F., & del-Pozo, F. (2013). HERMES: Towards an integrated toolbox to characterize functional and effective brain connectivity. *Neuroinformatics*, *11*, 405–434. doi:10.1007/s12021-013-9186-1

Olejarczyk, E., & Jernajczyk, W. (2017). Graph-based analysis of brain connectivity in schizophrenia. *PLoS One*, *12*, e0188629. doi:10.1371/journal.pone.0188629

Theodoridis, S., & Koutroumbas, K. (2008). *Pattern recognition*. Orlando, FL: Academic Press.

Theodoridis, S., Pikrakis, A., Koutroumbas, K., & Cavouras, D. (2010). *Introduction to pattern recognition: A Matlab approach*. Orlando, FL: Academic Press.

Tijms, B. M., Wink, A. M., de Haan, W., van der Flier, W. M., Stam, C. J., Scheltens, P., & Barkhof, F. (2013). Alzheimer's disease: Connecting findings from graph theoretical studies of brain networks. *Neurobiology of Aging*, *34*, 2023–2036. doi:10.1016/j.neurobiolaging.2013.02.020

Uddin, L. Q., Dajani, D. R., Voorhies, W., Bednarz, H., & Kana, R. K. (2017). Progress and roadblocks in the search for brain-based biomarkers of autism and attention-deficit/hyperactivity disorder. *Translational Psychiatry*, *7*, e1218–e1218. doi:10.1038/tp.2017.164

Wang, Y., Sokhadze, E., El-Baz, A., Li, X., Sears, L., Casanova, M., & Tasman, A. (2016). Relative power of specific EEG bands and their ratios during neurofeedback training in children with autism spectrum disorder. *Front. Hum. Neurosci.*, *9*.

Zwaigenbaum, L., & Penner, M. (2018). Autism spectrum disorder: Advances in diagnosis and evaluation. *BMJ*, *361*. doi:10.1136/bmj.k1674

Received September 18, 2020; accepted February 4, 2021.